

Ionization Potentials of Solids: The Importance of Vertex Corrections

Andreas Grüneis,¹ Georg Kresse,^{1,*} Yoyo Hinuma,² and Fumiyasu Oba^{2,3,†}

¹*Faculty of Physics and Center for Computational Materials Science, University of Vienna, Sensengasse 8/12, A-1090 Vienna, Austria*

²*Department of Materials Science and Engineering, Kyoto University, Kyoto 606-8501, Japan*

³*Materials Research Center for Element Strategy, Tokyo Institute of Technology, Yokohama 226-8503, Japan*

(Received 12 September 2013; published 7 March 2014)

The ionization potential is a fundamental key quantity with great relevance to diverse material properties. We find that state of the art methods based on density functional theory and simple diagrammatic approaches as commonly taken in the *GW* approximation predict the ionization potentials of semiconductors and insulators unsatisfactorily. Good agreement between theory and experiment is obtained only when diagrams resulting from the antisymmetry of the many-electron wave function are taken into account via vertex corrections in the self-energy. The present approach describes both localized and delocalized states accurately, making it ideally suited for a wide class of materials and processes.

DOI: 10.1103/PhysRevLett.112.096401

PACS numbers: 71.10.-w, 31.15.A-

Kohn-Sham density functional theory (DFT) is undeniably the workhorse theory of computational condensed matter physics and materials science. Although Kohn-Sham (KS) eigenenergies have in general no physical relevance and serve only as Lagrange multipliers conserving orthonormality of the orbitals, the eigenenergy of the highest occupied orbital or valence band maximum (VBM) is an exception. For the exact density functional, it corresponds to the vertical ionization potential (IP) [1,2], the energy required to remove an electron. This fundamental relation makes theoretical predictions of the IP particularly interesting, allowing one to address the quality of a given density functional. Furthermore, the IPs of semiconductors and insulators are of great practical relevance to the design of catalysts and photocatalysts. Among other things, they largely determine the natural band offsets between different materials that control the barriers for electron transport at heterojunctions in electronic devices and photovoltaic cells, as well as the electronic level alignment between molecules and surfaces. This clearly emphasizes that the IP is a property of paramount importance for the electronic behavior of materials.

Unfortunately, for any approximate, for instance, semilocal functional, the difference between the highest occupied KS eigenenergy and the experimental IP is often sizable. For molecular systems, hybrid functionals that mix the exact Hartree-Fock exchange with local or semilocal exchange-correlation functionals seem to yield slightly improved—but certainly not great—agreement with experiment (see, e.g., [3]). However, little is known for solids. As an alternative to KS DFT, one electron Green's function methods can be used to determine the IP, since the poles of the one-particle Green's function correspond to the electron addition and removal energies, and the smallest removal energy is just the IP. The Green's function is

usually calculated using a “perturbative” approach summing a certain set of Feynman diagrams. In solid state physics to date, the most common approximation is the random phase approximation (RPA) as used in Hedin's *GW* method. The RPA sums all electron-hole bubble diagrams to infinite order [4], but neglects ladder diagrams. It has been shown that inclusion of the electron-hole ladder diagrams in the screening, as also done in the Bethe-Salpeter approach to optical properties [5,6], is essential to reproduce experimental band gaps when self-consistent *GW* approaches or orbitals from hybrid functionals are used [7–9]. Very little, however, is known about the importance of the ladder diagrams in the self-energy, which are described by the vertex in Hedin's equations [4]. To date, these contributions have only been evaluated approximately, using DFT [10–12], neglecting the three-point nature of the vertex [13] or using approximations to the cumulant expansion [14,15]. The neglect of the three-point nature results in much too large band gaps, as also shown in the Supplemental Material [16]. Here, we introduce a novel three-point vertex for the self-energy. We show that it shifts delocalized states upwards towards the vacuum level but lowers localized states. This improves the IPs and the semicore *d* band positions significantly, indicating that the vertex corrected *GW* Γ approximation is required, when accurate predictions are needed for absolute quasiparticle (QP) energies, or whenever QP energy differences between localized and delocalized states are predicted.

The present ground-state calculations are based on generalized KS theory [17,18] and use either the Heyd-Scuseria-Ernzerhof (HSE) hybrid functional [19–21] or the Perdew-Burke-Ernzerhof (PBE) semilocal functional [22,23]. The IPs of nonpolar surfaces of semiconductors and insulators were determined on the level of KS theory, using the difference between the vacuum level and an electrostatic reference level in a bulklike region of surface

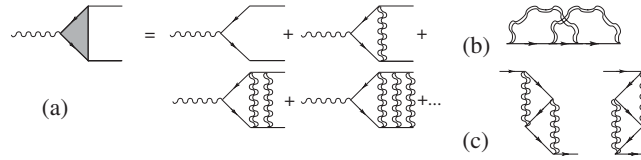


FIG. 1. (a) Vertex correction in the screened interaction $W^{\text{TC-TC}}$, and (b) and (c) first order vertex correction in the self-energy yielding the second order exchange diagram. (a) The incoming photon (wiggly line) creates a particle-hole pair (forward and backward arrows). The vertex describes the electrostatic interaction W (double-wiggly line) between the particles and holes. A static approximation is used for the screened interaction W (double-wiggly lines), as commonly done in solid state Bethe-Salpeter calculations [5]. Panel (c) corresponds to (b) but shows explicitly that time ordering gives rise to two second order exchange diagrams for a static W [compare two terms in Eq. (1)].

supercells, and the difference between the reference level and the VBM of bulk calculations [24]. The effect of spin-orbit coupling was included as a correction [16]. Slab and vacuum thicknesses were at least 18 Å. Atomic relaxation for the surfaces was conducted using PBE, and the lattice constants were then scaled to the experimental values for the IP evaluation. More details of the computational procedures can be found in the Supplemental Material [16].

The subsequent GW calculations were performed keeping the orbitals fixed, but determining the QP energies self-consistently. Keeping the orbitals fixed has the advantage that the Hartree potential remains identical to the ground-state KS calculations, and hence, the electrostatic alignment between the vacuum level and the bulk is fully determined by the KS ground-state surface calculations (HSE or PBE). Then, on the GW level, only fairly straightforward and efficient bulk calculations are required to determine the shift of the QP energies with respect to the original KS eigenenergies. On the level of GW , three progressively more accurate approximations were used. GW_0 @PBE is the most widely used approximation, in which the QP energies in the Green's function G are iteratively updated to self-consistency. The screened Coulomb interaction W_0 is determined using the RPA and PBE one-electron energy differences in the independent particle polarizability. The second level, $GW^{\text{TC-TC}}$ @HSE, is similar, but now the orbitals are from HSE calculations, vertex corrections are self-consistently included in W [compare Fig. 1(a)], and the QP energies are updated both in G and the independent particle polarizability (TC refers to test-charge). This approach yields very similar screening properties to the RPA with PBE one-electron energies (W_0 @PBE $\approx W^{\text{TC-TC}}$), but it is physically better justified: in the one-electron Green's function, the poles are now at the correct QP energies in close agreement with experiment, decreasing the screening. This is balanced by the included electrostatic electron-hole interaction (vertex in W), requiring the solution of the Bethe-Salpeter equation at each iteration. Except for no orbital update, this procedure is identical to that outlined in Ref. [8]. In the final step, we also include an approximate vertex in the self-energy, which properly closes the hierarchy, and is commonly referred to as $GW\Gamma$. Since inclusion of a fully frequency

dependent W in the vertex is computationally too demanding, we replace W by the “static” approximation $\lim_{\omega \rightarrow 0} W(\omega)$. This approximation is almost ubiquitously used for the solution of the Bethe-Salpeter equation and also adopted here for the ladder diagrams when $W^{\text{TC-TC}}$ or the self-energy is determined. Furthermore, we restrict ourselves to the second order time ordered diagrams shown in Fig. 1(c) with the algebraic expression for the QP energy shift of the occupied or unoccupied state \tilde{c} being

$$\Delta\epsilon_{\tilde{c}}(\omega) = \sum_{i,a,b} \frac{\langle i\tilde{c}|W|ab\rangle\langle i\tilde{c}|W|ba\rangle^*}{\epsilon_a + \epsilon_b - \epsilon_i - \omega} - \sum_{i,j,a} \frac{\langle ij|W|a\tilde{c}\rangle\langle ij|W|\tilde{c}a\rangle^*}{\epsilon_a + \omega - \epsilon_i - \epsilon_j}. \quad (1)$$

In Eq. (1), the integers i, j and a, b , respectively, denote occupied and unoccupied one-electron orbitals with QP energies $\epsilon_i, \dots, \epsilon_b$, and W is set to $W = W^{\text{TC-TC}}$. The additional contribution is added to the $GW^{\text{TC-TC}}$ @HSE quasiparticle energies, and we term this approximation $GW\Gamma^1$, since our vertex correction corresponds to the first order vertex $\Gamma(1, 2; 3) = G(1, 3)G(2, 3)W(1, 2)$ [25]. In the static approximation, the additional term is equivalent to the antisymmetric term in the second order QP energies, except for the replacement of the bare Coulomb interaction v by the statically screened Coulomb interaction W (see, e.g., Ref. [26]). Contributions to the QP renormalization (Z factor) can be computed but are generally found to be negligible. Furthermore, to account for the fact that single shot calculations are performed for the vertex contribution in the self-energy, the $GW\Gamma^1$ contribution is calculated neglecting the Z factor.

The GW and $GW\Gamma^1$ calculations were performed using projector augmented wave potentials [27] with approximately norm-conserving partial waves [16]. The Brillouin zone was sampled using $6 \times 6 \times 6$ k points for the GW calculations and $4 \times 4 \times 4$ k points for the contribution from Eq. (1). Convergence with respect to the unoccupied states has been carefully checked [28,29] by increasing the plane wave cutoffs to up to ~ 1250 eV for the GW calculations, including all unoccupied orbitals, and

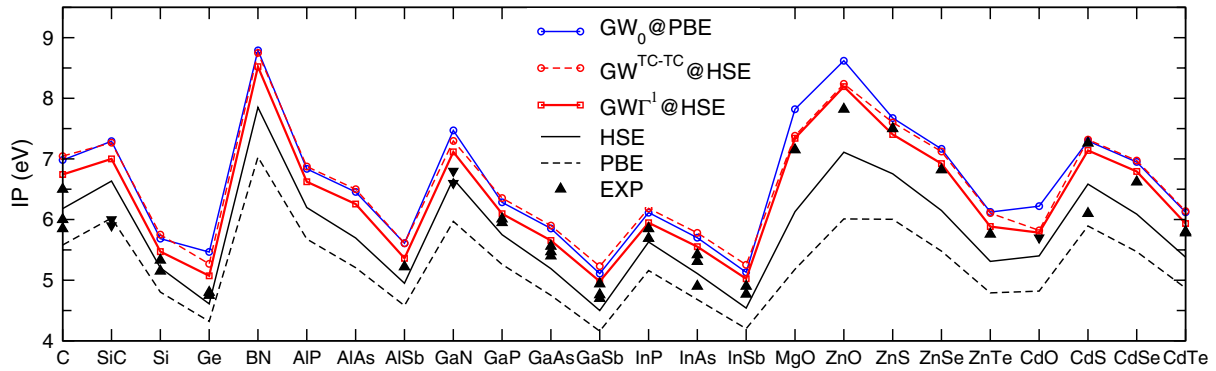


FIG. 2 (color online). Ionization potentials of various semiconductors and insulators obtained for nonpolar surfaces using PBE, HSE, GW_0 @PBE, GW^{TC-TC} @HSE, and $GW\Gamma^1$ @HSE [16]. Experimental (EXP) values for the corresponding nonpolar surfaces are shown with triangles, whereas those for different surface orientations are denoted by inverted triangles.

extrapolating to the infinite basis set limit [16]. The present calculations are significantly more accurate than previously reported ones using the same code [8,9].

Figure 2 shows the performance of the various approximations considered here. Comparison between theoretical and experimental IP values needs to be made carefully in view of the surface dependent nature of the IP [30]. Surfaces with the same orientation and reconstruction as those for available experimental data were used here, where nonpolar surfaces were chosen exclusively because polar surfaces can show complex, environment-dependent reconstructions. The considered structures are (111) 2×1 for C, Si, and Ge in the diamond structure, (11 $\bar{2}$ 0) for GaN and ZnO in the wurtzite structure, (100) for MgO and CdO in the rocksalt structure, and (110) for the rest of the compounds in the zinc-blende structure. The experimental IP values shown in Fig. 2 are for the corresponding surfaces, except for SiC with a polar, reconstructed (100) surface, GaN with a polar {0001} surface, and CdO, for which the surface orientation has not been specified [31–33].

Furthermore, surfaces subject to IP measurements might have been unintentionally contaminated, e.g., by hydrogen, which is difficult to detect and can cause a fairly large spread of the experimental values for some materials, such as diamond and CdS. Despite these obstacles, it is fairly clear that PBE yields on average 1 eV too small IPs. HSE increases the IPs by, on average, 0.6 eV, with larger enhancements for the oxides and large gap systems, substantially improving agreement with experiment. Overall, the performance of HSE is respectable, in particular, for the group IV and III–V semiconductors with errors mostly below 0.3 eV, although a sizable underestimation prevails for group II–VI compounds with wider band gaps. The performance of the standard GW_0 @PBE calculations is somewhat disappointing, and the IPs are generally too large. It is, furthermore, troublesome that the values predicted by HSE are significantly different from the GW_0 @PBE values. Which method should we trust? To

determine this, we are now stepping up the hierarchy of the diagrammatic methods.

With the exception of Ge and InAs (which are incorrectly described as metals by PBE), GaN, and the oxides, the IPs from the GW^{TC-TC} @HSE are almost identical to the GW_0 @PBE values. At first sight, this supports the much simpler GW_0 @PBE calculations. Obviously, the choice of the initial orbitals has only little effect on the final QP energies (note again that W_0 @PBE \approx W^{TC-TC} @HSE). We have also tested whether the choice of W influences the final results, and found that using GW_0 @HSE yields within 0.2 eV the same IPs as GW_0 @PBE, although the dielectric constants for W_0 @HSE are in error by about 30%. In summary, the theoretical QP IPs are rather robust and are influenced neither by the choice of the orbitals nor by the choice of the screened interaction W .

The next step is the inclusion of vertex corrections in the self-energy as already outlined above. From a diagrammatic point of view, the GW approximation does not include all second order diagrams in v , with the $GW\Gamma^1$ diagram shown in Fig. 1(b) being the next most important term. The corresponding “crossed” diagrams are related to the antisymmetry of the many-electron wave function, which is not properly accounted for by the standard GW approximation. Inclusion of these diagrams not only restores the antisymmetry of the underlying many-electron wave function but also removes self-interaction terms in the self-energy: a diagrammatic method becomes completely self-interaction free if all involved two electron four orbital integrals are antisymmetrized. Here, this is only achieved approximately to the second order in v and using a static approximation for W .

The effect on the QP energies is fortunately not very sizable, supporting the hope that order-by-order addition of screened diagrams might yield improved results with every increasing order. For most semiconductors, the $GW\Gamma^1$ self-energy correction shifts the valence band upwards and reduces the IP by approximately 0.2–0.3 eV. However, as we move towards earlier anions in a group, or towards more

TABLE I. Mean position of the semicore d states with respect to the VBM for HSE, $GW_0@PBE$, $GW^{TC-TC}@HSE$, and $GW\Gamma^1@HSE$, along with experimental values (in eV). The theoretical values were determined by averaging the d state energies at the Γ point. Since convergence of the d states is slow for $GW_0@PBE$, GW^{TC-TC} and $GW\Gamma^1$, errors are expected to be around 0.1 eV, despite extrapolation to the infinite basis set limit.

	HSE	$GW_0@PBE$	GW^{TC-TC}	$GW\Gamma^1$	Exp
ZnO	6.2	6.7	6.9	7.1	7.5
ZnS	7.6	8.1	8.0	8.4	9.0
ZnSe	8.0	8.3	8.2	8.6	9.2
ZnTe	8.6	8.9	8.8	9.3	9.8
CdO	7.5	8.6	8.5	8.7	8.8
CdS	8.6	9.1	9.1	9.5	9.5
CdSe	9.1	9.2	9.2	9.7	10.04
CdTe	9.3	9.7	9.7	10.2	10.5
GaN	15.6	16.8	16.6	17.0	17.0
GaP	16.9	17.9	17.8	18.3	18.55
GaAs	17.2	18.1	18.0	18.5	18.8
GaSb	17.5	18.5	18.2	18.7	19
InP	15.7	16.4	16.3	16.9	16.8
InAs	16.0	16.6	16.5	17.0	17.09
InSb	16.2	16.7	16.7	17.2	17.29

ionic materials, the shift becomes small (being practically zero for the oxides). To better understand this trend, we have also evaluated the position of the semicore d states using the four main approximations used in this Letter (Table I). The $GW\Gamma^1$ contribution shifts the d states down by approximately 0.5 eV, significantly improving agreement with experiment ($GW^{TC-TC} \rightarrow GW\Gamma^1$). We return to Eq. (1) to study this behavior. The equation can be considered as a variant of Koopmans' theorem describing the second-order exchange energy difference between the (N) electron system (first term) and ($N - 1$) system (second term) [34]. The first term leads to an increase and upward shift of the QP energy $\epsilon_{\tilde{c}}$, since the second-order exchange reduces the self-correlation energy of the (N) electron system. The second term partly corrects for the self-correlation of the now unoccupied orbital \tilde{c} in the ($N - 1$) electron system and results in a downward shift of the QP energy. In this term, the filled state index j can coincide with the considered state \tilde{c} . For strongly localized d states, this contribution becomes larger in magnitude than the first term, causing a downward shift of the corresponding QP energy by 0.2–0.6 eV. On the other hand, for very delocalized orbitals \tilde{c} , the second term on the rhs of Eq. (1) is small, and the first term prevails, shifting the QP energy upwards by 0.2–0.3 eV. As $GW\Gamma^1$ can be understood to reduce the self-interaction errors, the shifts are a clear indication that the standard GW approximation contains a sizable self-interaction error for delocalized as well as localized states. $GW\Gamma^1$ moves itinerant, bandlike states upwards towards the vacuum level and localized states in the opposite direction. It is gratifying that the resultant IPs

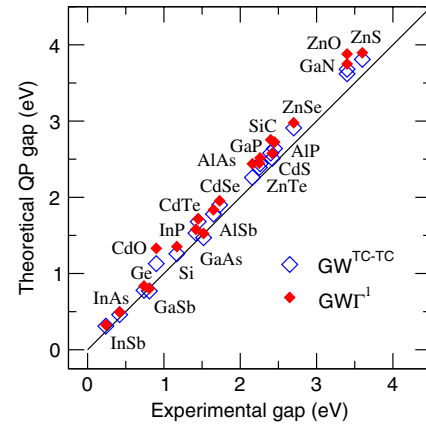


FIG. 3 (color online). Band gaps for $GW^{TC-TC}@HSE$ and $GW\Gamma^1@HSE$ versus experimental band gaps for the semiconductors considered in this work [16].

in the present $GW\Gamma^1$ calculations match the experimental data very well.

The final question to be addressed is whether the vertex in the self-energy changes the QP band gaps. As shown in Fig. 3, the effect is fairly small and typically less than 0.1 eV. In most semiconductors, the inclusion of the many-electron vertex in the self-energy shifts the valence and conduction band edges upwards by about 0.2 and 0.3 eV, respectively. Only for oxides and nitrides, the more localized valence band hardly moves when the self-energy vertex is included (compare IPs in Fig. 2), increasing the band gap slightly by 0.2 eV. The effect is most clearly visible for ZnO, CdO, and GaN, resolving the issue that most previous calculations for ZnO resulted in too small band gaps [29,35] even when fully self-consistent GW calculations were performed [8]. In the present case, the band gaps are now consistently too large with errors clearly and systematically decreasing from oxides, BN and carbon (0.4 eV) to semiconductors with heavier elements (GaAs, GaSb, InAs, InSb less than 0.05 eV). The residual error is partly related to the neglect of electron-phonon interactions, with estimated gap reductions of 0.1, 0.15, and 0.4 eV for Si [36], ZnO [37], and C [38], respectively, and lattice polarization contributions to the screening in polar materials [39]. We note that a more approximate diagrammatically constructed two-point vertex in the self-energy, as suggested in Ref. [13], yields much too large band gaps in particular for large gap ionic materials as shown in the Supplemental Material [16].

In summary, we have performed the first concise $GW\Gamma^1$ calculations, with a diagrammatic *ab initio* description of the vertex in both the screening and the self-energy. Inclusion of the vertex in the self-energy has important consequences. Dispersed states at the valence or conduction band edges shift upwards towards the vacuum level by up to 0.3 eV. This reduces the ionization potential compared to standard calculations without a vertex in the self-energy, yielding excellent agreement with

experiment. Since the shift is negligible for the more localized valence band states in oxides and nitrides, the standard *GW* approximation can not be used to predict accurate band offsets between diverse materials, for instance, at oxide semiconductor interfaces. Furthermore, the vertex in the self-energy shifts strongly localized states down by 0.5 eV, which is highly relevant for the description of electron and hole localization in polarons and defects and for the treatment of molecular levels on surfaces.

The present work establishes a method that allows one to calculate quasiparticle energies of both itinerant, bandlike states and localized states with a high degree of precision on an absolute scale. This constitutes a major breakthrough towards an accurate prediction of diverse processes involving polarons, point defects, pristine and adsorbate covered surfaces, interfaces, and hence, an efficient computational design of catalysts, photocatalysts, novel electronic devices, and photovoltaic cells.

This work was supported by the Austrian Science Fund (FWF) within the SFB ViCoM (Grant No. F 41), the Austrian Academy of Sciences within APART, the MEXT Elements Strategy Initiative to Form Core Research Center, and a Grant-in-Aid for Scientific Research on Innovative Areas (Grant No. 25106005) from JSPS. Supercomputing time on the Vienna Scientific cluster (VSC) and the ACCMS at Kyoto University is gratefully acknowledged.

*georg.kresse@univie.ac.at

†oba@cms.mtl.kyoto-u.ac.jp

- [1] J. P. Perdew, R. G. Parr, M. Levy, and J. L. Balduz, *Phys. Rev. Lett.* **49**, 1691 (1982).
- [2] J. P. Perdew and M. Levy, *Phys. Rev. Lett.* **51**, 1884 (1983).
- [3] M. J. van Setten, F. Weigend, and F. Evers, *J. Chem. Theory Comput.* **9**, 232 (2013).
- [4] L. Hedin, *Phys. Rev.* **139**, A796 (1965).
- [5] S. Albrecht, L. Reining, R. Del Sole, and G. Onida, *Phys. Rev. Lett.* **80**, 4510 (1998).
- [6] M. Rohlfing and S. G. Louie, *Phys. Rev. Lett.* **81**, 2312 (1998).
- [7] E. K. Chang, M. Rohlfing, and S. G. Louie, *Phys. Rev. Lett.* **85**, 2613 (2000).
- [8] M. Shishkin, M. Marsman, and G. Kresse, *Phys. Rev. Lett.* **99**, 246403 (2007).
- [9] J. Paier, M. Marsman, and G. Kresse, *Phys. Rev. B* **78**, 121201 (2008).
- [10] R. Del Sole, L. Reining, and R. W. Godby, *Phys. Rev. B* **49**, 8024 (1994).
- [11] A. Fleszar and W. Hanke, *Phys. Rev. B* **56**, 10228 (1997).
- [12] R. Shaltaf, G.-M. Rignanese, X. Gonze, F. Giustino, and A. Pasquarello, *Phys. Rev. Lett.* **100**, 186401 (2008).
- [13] F. Bruneval, F. Sottile, V. Olevano, R. Del Sole, and L. Reining, *Phys. Rev. Lett.* **94**, 186402 (2005).
- [14] F. Aryasetiawan, *Phys. Rev. B* **46**, 13051 (1992).
- [15] M. Guzzo, G. Lani, F. Sottile, P. Romaniello, M. Gatti, J. J. Kas, J. J. Rehr, M. G. Silly, F. Sirotti, and L. Reining, *Phys. Rev. Lett.* **107**, 166401 (2011).
- [16] See Supplemental Material at <http://link.aps.org/supplemental/10.1103/PhysRevLett.112.096401> for the computational details and the tabulated IP and band gap values.
- [17] T. L. Gilbert, *Phys. Rev. B* **12**, 2111 (1975).
- [18] A. Seidl, A. Görling, P. Vogl, J. A. Majewski, and M. Levy, *Phys. Rev. B* **53**, 3764 (1996).
- [19] J. Heyd, G. E. Scuseria, and M. Ernzerhof, *J. Chem. Phys.* **118**, 8207 (2003).
- [20] J. Heyd, G. E. Scuseria, and M. Ernzerhof, *J. Chem. Phys.* **124**, 219906 (2006).
- [21] A. V. Krugau, O. A. Vydrov, A. F. Izmaylov, and G. E. Scuseria, *J. Chem. Phys.* **125**, 224106 (2006).
- [22] J. P. Perdew, K. Burke, and M. Ernzerhof, *Phys. Rev. Lett.* **77**, 3865 (1996).
- [23] J. P. Perdew, K. Burke, and M. Ernzerhof, *Phys. Rev. Lett.* **78**, 1396 (1997).
- [24] Y. Hinuma, F. Oba, Y. Kumagai, and I. Tanaka, *Phys. Rev. B* **86**, 245433 (2012).
- [25] A. Schindlmayr and R. W. Godby, *Phys. Rev. Lett.* **80**, 1702 (1998).
- [26] A. Grüneis, M. Marsman, and G. Kresse, *J. Chem. Phys.* **133**, 074107 (2010).
- [27] P. E. Blöchl, *Phys. Rev. B* **50**, 17953 (1994).
- [28] B.-C. Shih, Y. Xue, P. Zhang, M. L. Cohen, and S. G. Louie, *Phys. Rev. Lett.* **105**, 146401 (2010).
- [29] C. Friedrich, M. C. Müller, and S. Blügel, *Phys. Rev. B* **83**, 081101 (2011).
- [30] D. Cahen and A. Kahn, *Adv. Mater.* **15**, 271 (2003).
- [31] W. Mönch, *Semiconductor Surfaces and Interfaces* (Springer, New York, 2001).
- [32] T. Jaouen, G. Jézéquel, G. Delhaye, B. Lépine, P. Turban, and P. Schieffer, *Appl. Phys. Lett.* **97**, 232104 (2010).
- [33] H. Hosono, *Transparent Electronics: from Synthesis to Applications*, (Wiley, New York, 2010), Chap. 2, p. 34.
- [34] A. Grüneis, M. Marsman, J. Harl, L. Schimka, and G. Kresse, *J. Chem. Phys.* **131**, 154115 (2009).
- [35] M. Shishkin and G. Kresse, *Phys. Rev. B* **75**, 235102 (2007).
- [36] P. Lautenschlager, P. B. Allen, and M. Cardona, *Phys. Rev. B* **31**, 2163 (1985).
- [37] S. Tsoi, X. Lu, A. K. Ramdas, H. Alawadhi, M. Grimsditch, M. Cardona, and R. Lauck, *Phys. Rev. B* **74**, 165203 (2006).
- [38] S. Poncecé, G. Antonius, P. Boulanger, E. Cannuccia, A. Marini, M. Coëté, and X. Gonze, *Comput. Mater. Sci.* **83**, 341 (2014).
- [39] S. Botti and M. A. L. Marques, *Phys. Rev. Lett.* **110**, 226404 (2013).